THE ASTROPHYSICAL JOURNAL, 419:136–149, 1993 December 10

SUBARCSECOND MID-INFRARED IMAGING OF WARM DUST IN THE NARROW-LINE REGION OF NGC 1068

MURRAY CAMERON
Max-Planck-Institut für extraterrestrische Physik, Giessenbachstraße, Postfach 1603, D-85740 Garching, Germany;
e-mail: cameron@mpe-garching.mpg.de

JOHN W. V. STOREY
School of Physics, University of New South Wales, P.O. Box 1, Kensington, New South Wales 2033, Australia

VALENTIN ROTACIUC, REINHARD GENZEL, LAURENT VERSTRAETE, AND SIEGFRIED DRAPATZ
Max-Planck-Institut für extraterrestrische Physik, Giessenbachstraße, Postfach 1603, D-85740 Garching, Germany

RALF SIEBENMORGEN
European Southern Observatory, Karl-Schwarzschild-Straße, D-85748 Garching, Germany

AND

TERRY J. LEE
Royal Observatory, Blackford Hill, Edinburgh EH9 3HJ, UK
Received 1993 March 22; accepted 1993 June 18

ABSTRACT

Subarcsecond 8 and 10 μm and diffraction-limited 19 μm imaging of the inner few hundred parsecs of the Seyfert nucleus in NGC 1068 shows the emission to be extended over a region of $\sim 70 \times 140$ pc. In particular, 10.3 μm images with spatial resolutions of 0".5 or better reveal that the warm dust is associated with the narrow-line clouds and is probably partially mixed with the photoionized gas. Extinction considerations, however, imply that the bulk of the warm dust is located deeper in neighboring molecular clouds, the exposed surfaces of which form the narrow-line clouds. Since there is little evidence for ongoing massive star formation in the narrow-line region, we argue that the mid-infrared emission arises from dust heated directly by radiation from the central nonthermal source. No single point source is observed to be responsible for more than $\sim 40\%$ of the 10.3 μm emission. The fact that the nucleus does not dominate the mid-infrared energy output from the nuclear environment is difficult to reconcile with current theories which incorporate a dusty, few parsec-scale molecular torus as the common agent unifying the two classes of Seyfert galaxies. This difficulty is further exacerbated by the observation that warm molecular gas is present in a region extending over 350 pc centered on the nucleus, and by the absence of a near-infrared excess in the spectrum which would indicate the presence of large column densities of hot dust close to the active galactic nucleus. As an alternative to the torus scenario, we present a model in which the molecular material in the nuclear vicinity is distributed in such a way that the bulk of the gas and dust lies at relatively large distances from the nucleus. In this case the line-of-sight extinction toward the broad-line region could be merely the result of one or more intervening molecular clouds. We demonstrate the plausibility of this scenario using a radiative transfer calculation for dusty clouds which incorporates scattering, an effect known to be important within ~ 100 pc of the nucleus.
Subject headings: dust, extinction — galaxies: individual (NGC 1068) — galaxies: ISM — galaxies: nuclei — galaxies: Seyfert — infrared: galaxies

1. INTRODUCTION

The nuclear regions of active galaxies, particularly of the Seyfert 2 genre, do not easily lend themselves to detailed observational scrutiny because of high and/or nonuniform extinction and the need for subarcsecond spatial resolution to distinguish components on scales of $\lesssim 100$ pc. Dust is less efficient at absorbing infrared photons than their optical counterparts, and, as a result, considerable efforts have been committed to infrared observations of active galactic nuclei (AGNs). Recently, near-infrared imaging spectrometers, offering both high spectral and spatial resolving powers, have started to provide a view of the molecular and ionized gas in the nuclear environments of such galaxies (Fischer, Smith, & Glaccum 1991; Rotaciuc et al. 1991; Genzel, Cameron, & Krabbe 1992; Blietz et al. 1994). In addition, the wide-field planetary camera (WFPC) on the *Hubble Space Telescope* (*HST*) has traced out the optically visible channel through which material is ejected from the nuclear vicinity (Evans et al. 1991). These data have reopened the question of the morphology of, and physical conditions in, the dusty environment that is believed to partially envelop and, in many cases, conceal the AGN. In particular, the presence of parsec-scale dust tori surrounding such nuclei, which forms the central plank of the unifying theory linking Seyfert types 1 and 2 (Krolik 1992), needs to be reexamined.

Grains at temperatures between 200 and 500 K radiate principally in the mid-infrared, and thus any body of dust, regardless of its detailed distribution, located close to an AGN may be traceable through its 5–20 μm emission. Application of this technique to the study of galactic nuclei has resulted in several $\sim 1''$ resolution images (e.g., Piña et al. 1992; Telesco & Gezari 1992; Keto et al. 1992). However, in the specific case of AGN studies, such imaging has not yet yielded useful limits on the extent of the emitting regions because selected targets have

been too distant to offer reasonable linear/angular scale ratios and/or the spatial resolution of the data has been inadequate. With sufficiently good spatial sampling of relatively nearby AGNs, mid-infrared observations could potentially provide the means to resolve several contradictory views, offered by X-ray, UV, and optical observations, of regions close to the active core. Specifically, any unifying model will have to account for the different extinction measurements highlighted by different lines, the high concentrations and spatial extents of both cold and warm molecular gas close to many nuclei, and the lack of observed near-infrared excesses in objects in which hot dust tori are thought to be present. Motivated by the need to address some of these issues, we selected NGC 1068 as our prime target during the commissioning of MIRACLE, the new MPE/ROE mid-IR camera.

This paper is structured as follows: in the remaining sections of this Introduction, we review relevant data on NGC 1068 as a prerequisite for placing the mid-infrared measurements in the context of a multiwavelength framework. In § 2 we describe our observing and data reduction strategy and present the results of these efforts. Section 3 deals with the possible mechanisms giving rise to the observed mid-infrared emission. Section 4 examines consequences of the presence of dust in narrow-line regions. Section 5 addresses inadequacies in current versions of the unifying model highlighted by these observations and concludes with the presentation of an alternative scenario.

1.1. *The Host Galaxy*

At a distance of 14.1 Mpc (Tully 1988) and with a far-infrared luminosity which ranks it among the brightest extragalactic sources observed with *IRAS* ($3 \times 10^{11}\ L_{\odot}$; Telesco & Harper 1980), NGC 1068 is a nearby, luminous, easily accessible and well-studied active galaxy, offering an equivalent linear scale of 68 pc arcsec^{-1}. The host galaxy is a Sb(*rs*)II spiral (Sandage & Tammann 1981), the disk of which is inclined by $\sim 20°$–$40°$ to the plane of the sky (Baldwin, Wilson, & Whittle 1987; Scoville et al. 1988). Although its notoriety stems chiefly from the presence of a highly energetic nonthermal nuclear source, NGC 1068 also harbors a starburst, located in the kiloparsec-radius molecular ringlike structure which surrounds the nucleus. A twin radio jet, originating close to the nucleus, extends outward to 13″ (Wilson & Ulvestad 1983) before apparently terminating in bow shocks (Wilson & Ulvestad 1987). On subarcsecond scales, the jet can be resolved into three or four individual components (the "nuclear radio triplet"), one of which may be coincident with the nucleus (van der Hulst, Hummel, & Dickey 1982; Wilson & Ulvestad 1983; Ulvestad, Neff, & Wilson 1987). Optical imaging spectroscopy has identified two distinct regions associated with highly excited ionized gas: a classical narrow-line region (NLR) of angular size ~6″ (Atherton, Reay, & Taylor 1985; Cecil, Bland, & Tully 1990; Evans et al. 1991) and an extended narrow-line region (ENLR) which pervades a large fraction of the disk out to ≥ 7 kpc (Sokolowski, Bland-Hawthorn, & Cecil 1991; Unger et al. 1992).

1.2. *The Infrared Nucleus*

Although it is often considered the prototypical Seyfert 2 galaxy, Antonucci & Miller (1985) discovered that optical polarized light from the nuclear region of NGC 1068 is dominated by broad Balmer and Fe II lines (FWHM ~ 3000 km s^{-1}), and, consequently, it appears that the galaxy possesses a Seyfert 1 nucleus which is concealed by an asymmetric dust distribution. This source of obscuration has been extensively modeled as a dense, dusty, few-parsec-diameter molecular torus which subtends a considerable solid angle as seen by the nucleus (Krolik & Begelman 1986, 1988; Awaki et al. 1991; Pier & Krolik 1992a). Typical torus geometries assumed by such models are 1.0 and 3.5 pc for the inner and outer radii, respectively, with a height of 1 pc above the equatorial plane (Balsara & Krolik 1993). The input hydrogen number density ranges from 10^3 cm^{-3} (Storchi-Bergmann, Mulchaey, & Wilson 1992) to 10^5 cm^{-3} (Pier & Krolik 1992b), with masses in the range 10^4–10^5 $M_{\odot}$, depending on the aspect ratio. Although optical speckle observations have been interpreted as indicating a ~2 pc component coincident with the nucleus in NGC 1068 (Meaburn et al. 1982), more recent measurements in the optical with the *HST* (Lynds et al. 1991), and in the near-IR utilizing speckle interferometry with both one (Chelli et al. 1987) and two (Hofmann et al. 1993) spatial dimensions, point to the presence of a larger (~0.″15 or ~10 pc) emitting region close to the AGN. Although the radial size of the torus proposed by Krolik & Begelman (1986) scales with source luminosity, thereby leading to predicted dimensions somewhat more consistent with the larger structure measured in NGC 1068, the need to maintain the observed Seyfert 1/Seyfert 2 ratio (Lawrence 1991) requires that the height of the obscuring phenomenon must be similarly scaled. However, it is unclear whether a dense torus with a height of a few parsecs above the equatorial plane, such as that proposed in current unifying models, could remain stable in close proximity to the gravitational field of an AGN. Near-infrared (1–5 μm) continuum emission generally traces cool stars and, to a lesser extent because of the relatively small column densities involved, the presence of hot ($T \sim 1000$ K) dust. However, it is as yet unclear what the near-infrared maximum in NGC 1068 represents: the nucleus is certainly obscured at wavelengths shorter than ~1 μm (Lebofsky, Rieke, & Kemp 1978) and, as suggested by the nondetection of broad Brα (DePoy 1987), probably out to at least 5 μm.

Since the energy output of the nuclear region of NGC 1068 peaks in the mid-IR at ~20 μm (Telesco et al. 1984), from simple blackbody arguments the medium dominating the emission from the nucleus of NGC 1068 must have a size $\gg 1$ pc (Phinney 1989). This circumnuclear material may be coincident with, or represent part of, one or more of the molecular clouds observed in the near-IR $S(1)$ $v = 1$–0 line of H_2 by Rotaciuc et al. (1991) and Tamura et al. (1991) and, with somewhat better spatial resolution, by Blietz et al. (1994), which they interpret as due to excitation in gas heated by intense X-ray radiation from the nuclear source (Rotaciuc et al. 1991) or shocks (Tamura et al. 1991). The detection of a cold molecular gas mass of 5×10^7 $M_{\odot}$ (scaled to 14.1 Mpc) in the inner 3″ (Planesas, Scoville, & Myers 1991) and the corresponding mapping of HCN (Tacconi et al. 1993) are further confirmation of a large concentration of material in the nuclear vicinity.

Previous mid-infrared (7–22 μm) observations of NGC 1068 have suggested that the thermally emitting region is extended over ~1″ (Becklin et al. 1973), that the intense flux is a consequence of hot dust emission (Lebofsky et al. 1978), that there is an additional, spatially distinct emitting region located ~1″ to the northeast (Tresch-Fienberg et al. 1987), and that a significant amount of the warm dust is located in the narrow-line region (Bailey et al. 1988). The most abundant sources of mid-infrared emission are dusty molecular clouds and circumstellar shells in which grains have been heated to a few hundred

degrees. The presence of a moderately deep 9.7 μm absorption feature attributed to silicates (Roche et al. 1991) and a corresponding emission feature at 19 μm (Lebofsky et al. 1978) is consistent with a warm dust origin for the mid-infrared emission from the nuclear environment. On larger scales, measurements of the thermal emission beyond the inner few hundred parsecs reveal that the total far-infrared luminosity is approximately evenly divided between the nucleus and the kiloparsec starburst ring (Telesco et al. 1984; Telesco & Decher 1988).

1.3. *The Infrared/X-Ray Connection*

In principle, knowledge of the X-ray spectra of the nuclear region of active galaxies should provide details of the nature of the obscuring and scattering material close to the central engines. The *Einstein Observatory* measured a relatively small soft (0.1–3.8 keV) X-ray flux (Monier & Halpern 1987), and hard (2–10 keV) X-ray emission was subsequently detected with *EXOSAT* (Elvis & Lawrence 1988). However, the higher spatial resolution offered by recent *ROSAT* observations (Wilson et al. 1992) suggests that the hard X-rays are most likely emitted predominantly by an extranuclear component. Hence, as suggested by Mulchaey, Mushotzky, & Weaver (1992), the line-of-sight extinction toward the nucleus of NGC 1068 is probably so great that even the hard X-ray emission, which can penetrate column densities of $\lesssim 10^{24}$ cm^{-2}, is totally suppressed. Accordingly, the molecular distribution observed in the infrared (Rotaciuc et al. 1991), one knot of which lies within 0.″3 of the nucleus and which corresponds to a column density of $\sim 10^{23}$–10^{24} cm^{-2} (Cameron et al. 1993; Blietz et al. 1994), could plausibly be a major contributor to the X-ray extinction. If NGC 1068 does indeed harbor a Seyfert 1 nucleus, then this level of attenuation may explain its low X-ray luminosity.

Unifying models predict that the electron cloud thought responsible for the X-ray, optical, and, possibly, near-infrared scattering should be confined to a region close to, but above, an optically thick torus (Antonucci & Miller 1985). However, attempts to locate such a supposedly compact medium have proved unsuccessful (Caganoff et al. 1991), probably implying that this component is extended on the $\geq 1''$ scale (Antonucci 1992). An additional complication for the unifying theory is that the energy input needed to maintain the observed level of ionization in the outflow cone is considerably greater than the bolometric luminosity measured for the AGN in NGC 1068 (Miller, Goodrich, & Mathews 1991).

As a result of these various observational and theoretical discrepancies, a comprehensive and self-consistent picture of the inner few hundred parsecs of NGC 1068 is lacking. Here we present a series of high spatial resolution mid-IR images which offer insight into the nature of the circumnuclear dust regime and cast doubt on aspects of currently popular unifying models.

2. OBSERVATIONS

We used the MPE/ROE mid-IR camera, MIRACLE, to observe the central region of NGC 1068 during the instrument's commissioning at the 3.8 m United Kingdom Infrared Telescope (UKIRT) on the nights of 1991 November 1, 2, 5, and 6. MIRACLE is a joint venture between the Max-Planck-Institut für extraterrestrische Physik (MPE) and the Royal Observatory Edinburgh (ROE) to develop a 7–22 μm imaging system, based on a 62 × 58 pixel Si:As array supplied by the Santa Barbara Research Center. At the f/35 focus of UKIRT, MIRACLE offers an image scale of 0.″17 pixel^{-1}, resulting in a field of view of $\sim 10''$ and threefold oversampling of the diffraction spot (0.″55 at 10 μm at UKIRT). Excluding the outermost strip of guard ring pixels, the array contains no dead detectors. Data can be acquired through a selection of broad- and narrow-band 10 and 20 μm filters and a 7–14 μm circular variable filter [CVF; $R = (\lambda/\Delta\lambda) \gtrsim 50$] which are mounted on a remotely controlled wheel located in the Dewar. The readout of the array, filter selection, movement of the secondary mirror during chopping, and all data acquisition tasks are handled by a dedicated VME computer. A more detailed description of this system is given by Cameron et al. (1992).

NGC 1068 was observed with the CVF at 7.8 μm ($R = 70$) and two $R = 100$ filters centered at 10.3 and 18.7 μm. The sensitivities of the system for a 10 σ detection of a diffraction-limited point source in 10 minutes through these three filters are 250, 330, and 970 mJy, respectively. The use of a relatively narrow filter at 10.3 μm avoided contamination by the silicate absorption feature and the 10.5 μm [S IV] fine-structure line. Although broader band filters would, in theory, deliver significant improvements in sensitivity, this turns out not to be the case in reality (Cameron et al. 1992). A typical observing sequence involved focusing and calibrating on a nearby standard star, then acquiring and tracking the optical imaging of NGC 1068 using the UKIRT guide camera. Sequences of 10 s integrations were accumulated by reading out the array at 30 or 60 Hz while chopping at a frequency of a few hertz. Chop throws varied from 6″ to 40″, the advantage of the former being that both the positive and the negative beams were present simultaneously on the array, thus increasing the observing efficiency. However, it is known that about 20% of the total mid-IR flux of NGC 1068 arises in a disk which extends beyond 5″ (Telesco & Decher 1988). This diffuse extended emission is relatively uniform and should not have affected the morphology in the short chop throw images. As a control, during reduction we treated data obtained with the two chop throws separately. From comparison of these two sets of measurements we conclude that there are no differences between images obtained with different chop throws. Beam switching was typically performed after every 50 s of on-source integration, and standard stars were regularly observed to check seeing, focusing, and calibration.

Data reduction was carried out within the MIDAS environment. Prevailing weather conditions were such that, particularly for the 20 μm data, several data sets were discarded because of poor transmission. Each 50 s sequence of data was treated separately, and, in addition, for data obtained in short chop throw mode, the positive and negative beams were extracted and handled independently. To correct for small pointing shifts and to combine images in which the source had been positioned in different parts of the array, a two-dimensional Gaussian was fitted to each data sequence to determine the position of the maximum. For data obtained through each filter, individual sequences were then shifted to the nearest tenth of a pixel and co-added. The instrument/telescope beam profile shows a slight east-west elongation, probably resulting from the positioning accuracy of the secondary mirror during chopping and/or focusing effects. The total on-source integration times were 500, 2530, and 600 s for the 7.8, 10.3, and 18.7 μm data, respectively. Conditions during the observing period were somewhat less than optimum, and we have therefore been unable to obtain accurate photometry. However, many spectrophotometric data are available for

TABLE 1

DETAILS OF THE MIRACLE MEASUREMENTS OF NGC 1068

Date 1991	λ (μm)	$\Delta\lambda/\lambda$ (%)	t_{int} (s)	$FWHM_{NGC1068}$[a]	$FWHM_{PSF}$[b]
Nov 1.....	10.3	1.0	1630	1".3 × 1".3	1".0 × 0".7
Nov 5.....	10.3	1.0	900	1.3 × 1.1	1.3 × 0.9
Nov 5.....	7.8	1.4	500	1.2 × 1.1	1.0 × 1.0
Nov 6.....	18.7	1.0	600	1.2 × 1.1	1.2 × 1.0

[a] Values for the FWHM are measured along the major and minor axes.

[b] FWHM values for the PSFs refer to those measured along the right ascension and declination axes, respectively. Note, however, that the position angles of the mid-IR emission from NGC 1068 and the standard stars are not identical, since the latter arises from a slight east-west elongation of the PSF.

NGC 1068, from which we determine that the nuclear flux is 16, 18 (Kleinmann, Gillett, & Wright 1976; Cutri et al. 1981), and 70 Jy (Lebofsky et al. 1978) at 7.8, 10.3, and 18.9 μm, respectively.

2.1. *Spatial Distribution of the Mid-IR Emission*

Table 1 gives details of the characteristics of each data set and their corresponding measured beams. At 7.8 and 10.3 μm the point-spread function (PSF) is dominated by seeing effects, whereas at 18.7 μm the size of the diffraction spot is the most significant contributor. Corresponding images are shown in Figure 1. Although the 8 and 10 μm images are just resolved in terms of FWHM, the 10 μm measurements go sufficiently deep to highlight emission extending $\geq 1''$. Such faint extended emission cannot be detected in the data of Tresch-Fienberg et al. (1987), probably owing to a combination of lower signal-to-noise ratio (S/N) (their peak S/N is a factor of 2 lower), poorer spatial sampling, and larger beam profiles (2".3 × 1".3). Except for the data obtained at 18.7 μm, our mid-IR images of NGC 1068 are elongated to the northeast. In addition, the 10.3 μm images also show an extension to the southwest which is either absent or, at most, only hinted at in the 7.8 μm image. This discrepancy, and the fact that the 18.7 μm image appears unresolved, can almost certainly be ascribed to signal-to-noise effects.

Two distinct components can be clearly differentiated in our highest S/N 10.3 μm image (Fig. 1*a*), namely, a bright unresolved core and a region of extended diffuse emission, elongated northeast to southwest. As a means of better distinguishing the various components in this image, we have applied a Lucy-Richardson spatial resolution enhancement algorithm (Richardson 1972; Lucy 1974). These MIRACLE data are particularly well suited to such treatment because of the good spatial sampling of the PSF. This sampling is such that in all cases the beam FWHM is spread over $\gg 20$ pixels. Because the data obtained through the 10.3 μm filter on 1991 November 1 and 5 have rather different associated beams and

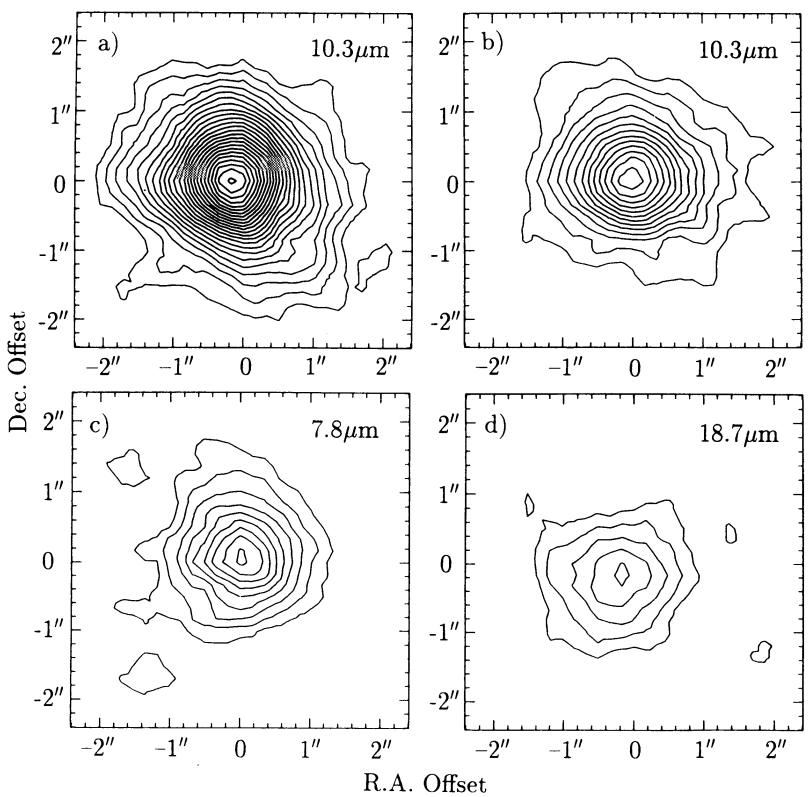

FIG. 1.—The nuclear region of NGC 1068 as imaged in the mid-infrared with MIRACLE. The plate scale of MIRACLE is 0".17 pixel^{-1}. In all cases the lowest contour represents the 1 σ pixel^{-1} level, increasing with 1 σ pixel^{-1} steps. The various images have been arranged so that the peak corresponds to (0, 0). (*a*) 10.3 μm image obtained on 1991 November 1. The bandwidth of the filter was 1%. The lowest contour level corresponds to 300 mJy arcsec^{-2}, and the peak represents a 28 σ pixel^{-1} detection. (*b*) As in (*a*), except that these data were obtained on November 5 and the beam shape is somewhat different. The lowest contour corresponds to 550 mJy arcsec^{-2}, and the flux peak represents a 15 σ pixel^{-1} detection. (*c*) 7.8 μm image obtained using the CVF with a bandwidth of 1.4%. The lowest contour corresponds to 1.0 Jy arcsec^{-2}, and the peak represents a signal-to-noise ratio of 9. (*d*) 18.7 μm image measured with a 1% filter. The lowest contour corresponds to 7.5 Jy arcsec^{-2}, and the peak represents a signal-to-noise ratio of 6.

signal-to-noise ratios, we treated these two data sets separately. The resulting deconvolved images have been convolved to an effective resolution of ~0".5 for the November 1 10.3 μm data and ~0".7 for all other data, corresponding to ~34 and 48 pc, respectively. As a check, all resulting frames were convolved with their corresponding original beams, revealing no significant discrepancies.

The resulting deconvolved images, presented in Figure 2, represent the sharpest mid-IR images yet obtained of an AGN and allow us to probe the emission on hitherto unmatched spatial scales. It is clear that these data offer somewhat different impressions of the nuclear region. However, we emphasize that the spatial resolution of images which result from the application of such deconvolution algorithms is a strong function of the signal-to-noise ratio at each position in the input frame. The higher spatial resolution obtained for Figure 2*a* merely reflects the greater S/N of the raw data in this case. As would be expected from inspection of Figure 1*d*, deconvolution of the 18.7 μm data does not provide additional information on the spatial distribution of the emission, owing to the poor S/N. All of the other three images in Figures 2*a*–2*c* show an elongation to the northeast of a bright point source, although the position angle in the 7.8 μm data is slightly greater than that in the other two frames. Our opinion that these data sets are wholly consistent is supported by the fact that all the deconvolved data show essentially the same structure in those areas of the original frames in which the S/N was highest.

Although the unresolved core in our 0".5 10.3 μm data is certainly the brightest feature in this image, it only accounts for ~30%–40% of the total mid-infrared flux from the central regions of NGC 1068. Tresch-Fienberg et al. (1987) determined that the mid-IR emission from the nuclear environment arises in two point sources: one located at the nucleus and the other 1"–2" to the northeast. The higher resolution MIRACLE data reveal a far more complex morphology, in which the bulk of the emission arises beyond the central peak, but still from a region only ~2" (140 pc) in extent. From this map it is clear that, regardless of its actual registration, the environment within ~35 pc of the nucleus does not dominate the warm dust emission. Further, the fact that the emission is extended over ~140 pc requires the presence of either a substantial number of localized heating sources or a less enshrouded AGN than has been previously postulated.

2.2. *Pinpointing the AGN*

Although it is intructive to compare the distribution of the mid-IR emission with that obtained at optical and radio wavelengths where the spatial resolution is similarly better than 1", we must first address the question of where to locate the nucleus in each case, as a means of effectively registering different images. Registration of the *HST* [O III] image (Evans et al. 1991) with VLBI data (Ulvestad et al. 1987) suggests that the apex of the narrow-line cloud illuminated conical cavity, which likely originates close to the AGN core, is coincident with the most southerly, and weakest, component of the nuclear radio triplet source (Evans et al. 1991). However, the astrometric uncertainty in aligning these two images is ~0".7 (~48 pc), and the registration adopted by Evans et al. (1991) is heavily dependent on the assumption that a conical surface can be fitted to the apparent positions of the [O III] emitting clouds. Given the fact that extinction may play a role in determining, at least partially, our view of the NLR , it is unclear with what accuracy the apex of this cone, and hence the location of the AGN,

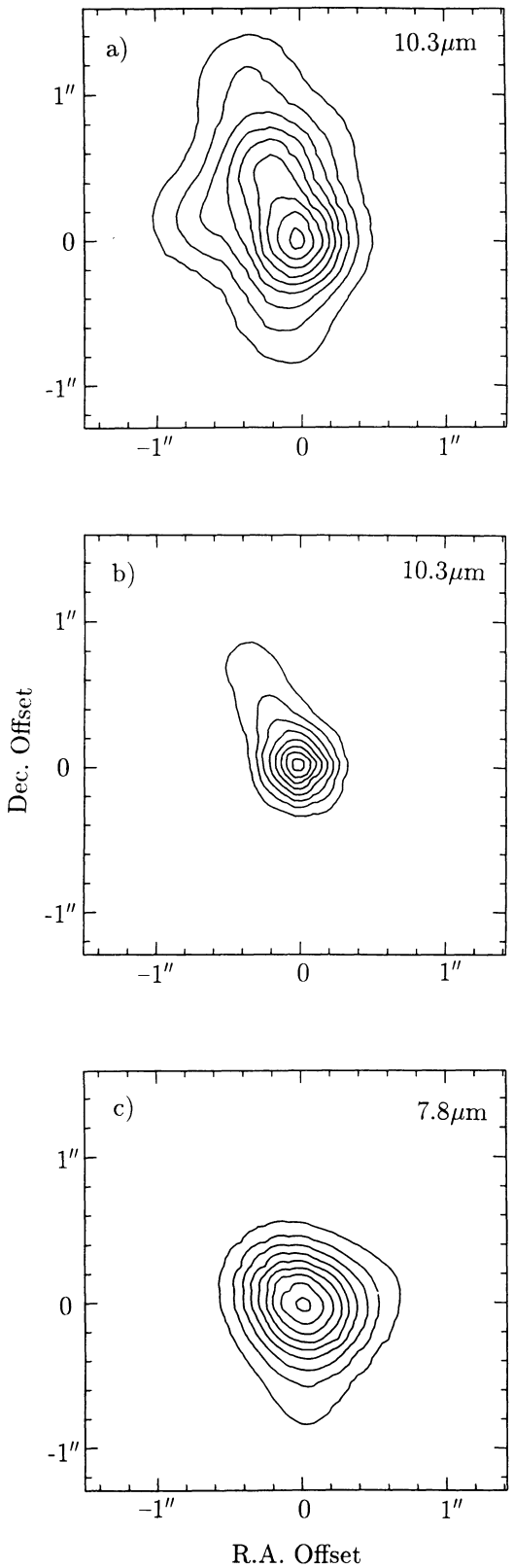

FIG. 2.—Data obtained at (*a*) 10.3 (Nov 1), (*b*) 10.3 (Nov 5), and (*c*) 7.8 μm deconvolved with their respective beams using a Lucy-Richardson algorithm. The resulting images have effective FWHMs of ~0".5 in the case of (*a*) and ~0".7 for (*b*) and (*c*). In each case the lowest contour corresponds to 10% of the flux in the peak pixel, with subsequent contours representing 20%, 30%, ...

can be registered on optical images. However, the basic proposal that the AGN is probably not coincident with the brightest radio component is supported by radio interferometry measurements (Planesas et al. 1991). The peak in the *HST* continuum image (Lynds et al. 1991) apparently lies a mere 0".05 (~3 pc) from the location of the nucleus as determined by Evans et al. (1991). Such a displacement is consistent with the offset between the near-IR continuum peak and the maximum in the 2.12 μm H_2 emission (0".2 $\pm$ 0".3; Blietz et al. 1994), although the coincidence between the optical and 2 μm continuum peaks has only been determined with an accuracy of $\pm$0".4 (Gallais 1991). Braatz et al. (1992) have estimated an offset of 0".5 $\pm$ 0".2 between the peak in their 12.4 μm image of NGC 1068 and the maximum in the visible. This displacement is considerably greater than those measured between the optical and any other wavelength. However, caution needs to be exercised in considering offsets determined between data sets obtained at very different angular resolutions. Accordingly, the magnitudes of these various uncertainties and the fact that much hinges on the accuracy of tracing out the profile of the conical outflow cavity imply that registration of radio, optical, and infrared images cannot realistically be achieved to better than ~0".3–0".5.

For registration of our MIRACLE map we assume that the maximum in the mid-infrared will arise from material close to the nucleus. The central engine is undoubtedly the origin of an intense radiation field, and since extinction toward this region is sufficient to attenuate directly observable X-ray, optical, and near-IR emission from the broad-line region, it is likely that the most intense dust emission arises close to the nucleus. This might not be the case if the 10 μm emission were affected by radiative transport effects within the circumnuclear molecular disklike structure. Dust becomes optically thick to 10 μm radiation at column densities in exces of $\sim 3.4 \times 10^{22}$ cm^{-2} ($A_V \sim$ 18; Cardelli, Clayton, & Mathis 1989). Although the optical depth of the silicate absorption feature at 9.7 μm is less than unity ($\tau_{9.7\mu m} = 0.56$; Roche et al. 1984), suggesting that transfer effects may not play an important role, such low estimates of the prevailing hydrogen column densities run contrary to those determined from the observed lack of hard X-ray emission. However, the extinction elucidated from the silicate absorption may arise in the cooler outer dusty regions of the circumnuclear disk, where the column density is lower, while the X-rays are probably attenuated in a region, characterized by a higher filling factor, lying closer to the AGN. Nevertheless, although the mid-IR emission associated with the immediate vicinity of the nucleus is almost certainly affected by radiative transport, it is difficult to conceive of a geometry which would displace the peak by more than a few tenths of an arcsecond from the AGN.

2.3. *Comparison with Optical and Radio Maps*

As a means of determining the relationship between the mid-infrared emitting agents and those giving rise to other phenomena, we have carried out comparisons with data sets offering similarly high spatial resolution, namely, the optical *HST* maps of Lynds et al. (1991) and Evans et al. (1991) and the 1.3 cm radio image of Ulvestad et al. (1987). The *HST* optical continuum map of Lynds et al. (1991), which is dominated by a core embedded in a more diffuse emitting region, bears little relationship to the mid-infrared emission at a resolution of 0".5. Since the extended optical continuum map appears to be dominated by stellar light, the apparent lack of correlation between the 5500 Å and 10.3 μm emitting components suggests that stars are not the energy source(s) of the mid-infrared emission. The better correlation between the 5007 Å *HST* map of the [O III] line, which traces clouds in the narrow-line region, led us to convolve the maximum entropy method (MEM) corrected data of Evans et al. (1991) to the resolution of our 10.3 μm data. A comparison of these data is presented in Figure 3 (Plate 1) from which it is clear that the two emitting regions are closely correlated. The good signal-to-noise quality of our deepest 10.3 μm map (Fig. 1*a*; $S/N_{source} \sim 120$, $S/N_{peak\ pixel} \sim$ 27) allows us to extend the deconvolution process somewhat further than that resulting in Figure 3. Figure 4 (Plate 1) shows our MIRACLE map and the *HST* [O III] map convolved to a resolution of 0".34 in which each resolution element is sampled by 4 pixels. It should be emphasized that the resulting distribution shown in this map is a strong function of the signal-to-noise ratio in the original data. The registration in Figure 4 has been achieved by means of a cross-correlation algorithm, and thus a degree of caution needs to be exercised when interpreting the alignment of these 0".34 resolution images. However, since the registration uncertainty cannot be more than a few 0".1, the striking similarity between the distribution of warm dust and the narrow-line clouds revealed by Figure 4 lends significant support to the hypothesis that these two emitting agents are intimately related.

The dust delineated by our mid-infrared observations may be located in one or more of three zones in the nuclear vicinity: the broad-line region (BLR), a circumnuclear torus, and the narrow-line region. The size of a typical BLR, R_{BLR}, scales with the bolometric luminosity as $R_{BLR} = 0.02 L_{45}^{0.5}$ pc, where the luminosity is expressed in units of 10^{45} ergs s^{-1} (Netzer 1990). Given that the predicted dust temperature at such small distances from the AGN (see § 3.3) would exceed that required for grain sublimation, it is unlikely that dust mixed with the broad-line clouds could survive the intense radiation field. That a few parsec-scale circumnuclear tori could be responsible for the dust emission seen to arise close to the nucleus cannot be ruled out, but its postulated enshroudment role is difficult to reconcile with the extended distribution seen in our 10.3 μm map as well as with other measurements. This a subject that will be addressed more fully in § 5. The striking similarity between the mid-infrared continuum and [O III] line emission implies the presence of large column densities of hot dust in the narrow-line region of NGC 1068. Although previous optical and infrared spectroscopy has suggested that the NLR in NGC 1068 may not be dust-free (Bailey et al. 1988; Goodrich 1992), these MIRACLE data are the first conclusive evidence for a large amount of dust associated with the narrow-line clouds. Figure 3 is remarkable in that it implies that dust is being heated to several hundred kelvins over a region 140 pc in extent, yet the nucleus, which according to current unifying theories should dominate the 10.3 μm emission (Pier & Krolik 1992b), is merely a minority, although admittedly still important, contributor to the total mid-infrared output. Evans et al. (1991) have already pointed to the correspondence between the locations of several of the narrow-line clouds and the components of the radio triplet source. By implication, such a relationship also holds for the mid-infrared emission.

The registration in Figure 3 highlights the asymmetry in the warm dust emission, probably because the emitting regions are almost exclusively located on the northern side of the nucleus. Intrinsically one-sided emission is also a feature of the *HST*

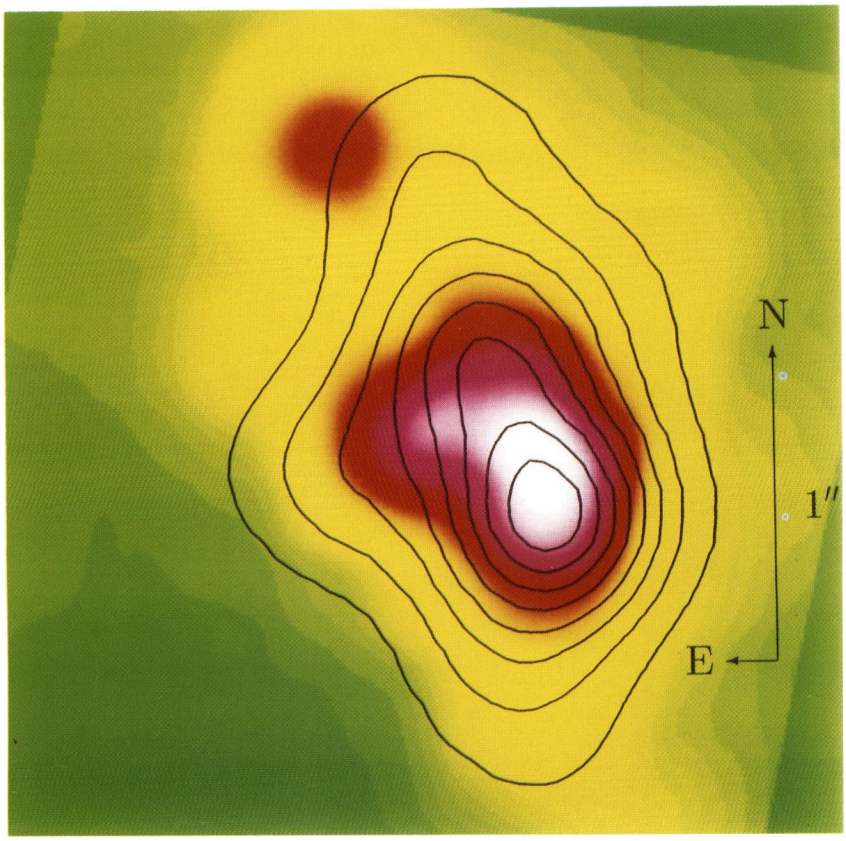

FIG. 3

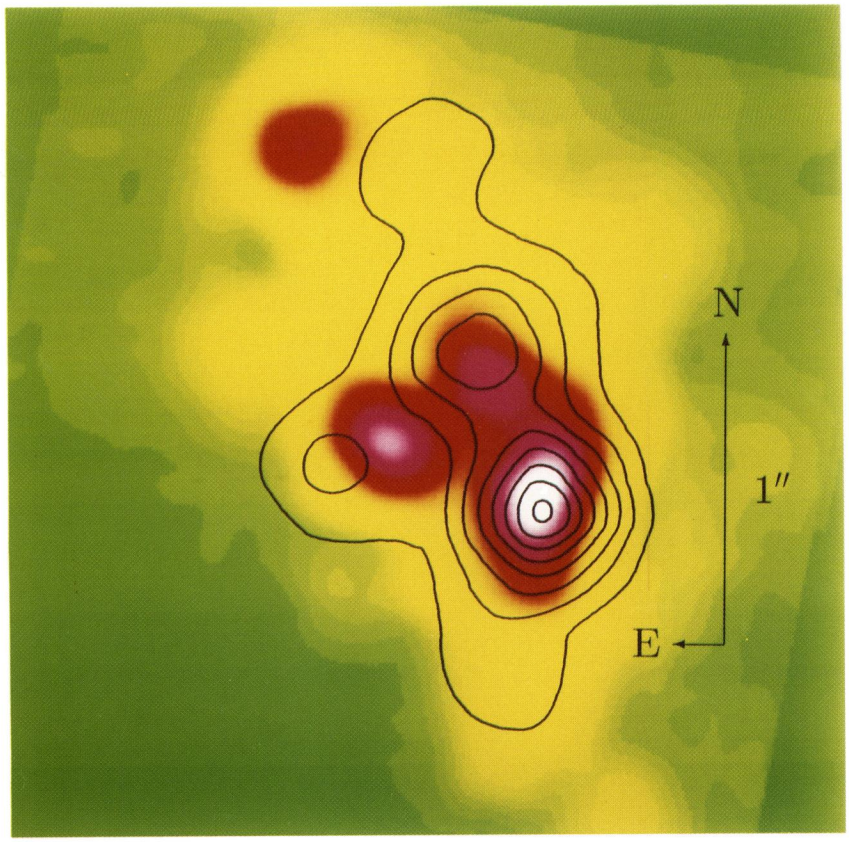

FIG. 4

FIG. 3.—Contour plot of the MIRACLE 10.3 μm map overlaid on a color version of the MEM-corrected *HST* [O III] image of the narrow-line region in NGC 1068 (Evans et al. 1991), both at an angular resolution of 0.″5. Contour levels as for Fig. 2.

FIG. 4.—As in Fig. 3, except that both the contour plot of the 10.3 μm image and the color version of the *HST* [O III] data are displayed with effective angular resolutions of 0.″34.

map of the narrow-line region (Evans et al. 1991). In contrast to the case of the [O III] imaging, the apparent lack of bipolarity in the 10.3 μm data cannot simply result from velocity shifting of an emission line out of the filter bandpass. Although such effects could be attributed to the presence of the molecular disklike structure, which, because of our viewing angle, may obscure optical and infrared emission south of the nucleus, extinction cannot be invoked, since the observed asymmetry is also a feature of the radio emission. In fact, on opposite sides of the nucleus the radio emission displays an entirely different morphology on both subarcsecond (Ulvestad et al. 1987) and larger (Wilson & Ulvestad 1983) scales. On the southern side close to the nucleus the emission is weak or absent, while the counterpart of the northern jet shows little indication of collimation. Such a situation would arise if the molecular cloud distribution exhibited intrinsical asymmetry, with the bulk of the material located to the north of the nucleus. The absence of mid-IR emission to the south would then be a consequence of the lower column density of dusty clouds in that direction. There is some support for this suggestion in that the distribution of warm H_2 observed in the near-IR appears to be predominantly associated with the northern part of the jet (Cameron et al. 1993; Blietz et al. 1994). The extreme diffuse morphology of the radio emission to the southwest of the nucleus might then be the result of insufficient molecular material capable of forming a buffer zone which could naturally collimate the outflowing gas. The apparent asymmetry in NGC 1068 has its parallel in the molecular cloud distribution in our own Galactic center (e.g., Bally et al. 1987).

3. POSSIBLE MECHANISMS PRODUCING THE MID-INFRARED EMISSION

Bearing in mind the spatial relationship between the distribution of the hot dust, narrow-line clouds, and radio emitting features, three possible mechanisms could be responsible for heating dust extended over 100 pc to such high temperatures, namely, extended star-forming regions, shocks and radiation from the nuclear accretion disk. We now examine each of these mechanisms in the light of available observational evidence.

3.1. *Heating by Massive Stars*

The scenario that star formation is active within the inner few kiloparsecs of the nucleus of NGC 1068 has been invoked to explain various phenomena (Telesco et al. 1984; Balick & Heckman 1985; Baldwin et al. 1987; Bruhweiler, Truong, & Altner 1991). It has been well established that NGC 1068 is passing through a starburst phase (Wynn-Williams, Becklin, & Scoville 1985), at least in the kiloparsec-radius molecular structure surrounding the nucleus, but apart from some controversy over the origin of the nuclear radio triplet (van der Hulst et al. 1982; Wilson & Ulvestad 1983), there is scant evidence for extensive star formation activity in the nuclear environment. This is consistent with the observed high level of ionization in the conical cavity (Pogge 1988), which suggests that the energetics in this region are dominated by the nonthermal continuum source. Additional supporting evidence comes from the *HST* spectrum of the optical/near-IR nucleus (Caganoff et al. 1991), which points to a [O III] λ5007/Hβ ratio indicative of photoionization by a power-law continuum source rather than excitation by young stars (Baldwin et al. 1987; Veilleux & Osterbrock 1987). In addition, the optical spectrum of the nuclear region of NGC 1068 shows no evidence for the presence of stars of type earlier than F (Koski 1978), while analysis of UV multiaperture data suggests that the observed shock-excited lines cannot arise from starburst activity close to the nucleus (Kriss et al. 1992). Hence it appears unlikely that, in the absence of a large contingent of massive young stars, the extended warm dust distribution can be heated by circumnuclear star formation.

3.2. *Dust Heated in Shocks*

Alternatively, dust may be heated by shocks in the nuclear vicinity. Indeed, on the basis of ultraviolet spectroscopy in the central region of NGC 1068, Kriss et al. (1992) argue that the emitting gas is excited partly in shocks triggered by the radio jet. The correspondence between some of the [O III] emitting clouds of Evans et al. (1991) and the radio knots of Ulvestad et al. (1987) lends further support to this idea, as does the similarity between the distribution of the [Fe II] emitting agent and the radio jet (Blietz et al. 1994).

In the case of a face-on shock, the dust emission flux is given by (Draine 1981)

$$\lambda I_\lambda = 5.5 \times 10^{-12} \left(\frac{n_{\rm H}^0}{10^4\ {\rm cm}^{-3}}\right)\left(\frac{v_s}{300\ {\rm km\ s}^{-1}}\right)^3 \times \left(\frac{\phi}{10^{-2}}\right)\left(\frac{\Omega}{\rm arcsec^2}\right) {\rm ergs\ cm}^{-2}\ {\rm s}^{-1}\ , \quad (1)$$

where $n_{\rm H}^0$ and v_s represent the preshock density and shock velocity, respectively; ϕ is the volume filling factor of the dusty clouds; and Ω is the solid angle of the emitting region. The clouds traced by [O III] λ5007 (Evans et al. 1991) imply $\phi \sim 10^{-2}$, a value typical of narrow-line regions (Osterbrock 1991). For a NLR of radius 300 pc and a cloud mean size of 10 pc, this value of ϕ corresponds to a surface covering factor of $\sim$0.1, consistent with observations (Netzer 1990). From spectrophotometry of the optical continuum peak, Caganoff et al. (1991) derive a density of 1200 cm^{-3} for the emitting material but argue that the gas must be denser in order to keep a significant fraction of the oxygen in the [O III] state. Cecil et al. (1990) have inferred a somewhat higher value ($n_e \sim 3 \times 10^4$ cm^{-3}), and we shall adopt this as being representative. Kriss et al. (1992) argue that the observed UV emission lines can be accounted for with a composite model involving both power-law continuum and shock excitation, with $v_s = 160$ km s^{-1}. However, comparison of their line ratios with the models of Viegas-Aldrovandi & Contini (1989) would lead to larger values of $v_s \sim 300$ km s^{-1}. We therefore adopt this latter value as an upper limit. From our 10 μm data we can determine that a generous upper limit to the solid angle of the emitting region is 2 arcsec^2. The energy radiated by dust in such a favorably viewed shock would be $\sim 2 \times 10^{-11}$ ergs s^{-1} cm^{-2}, almost four orders of magnitude less than the flux actually emitted by the nucleus. It thus appears unlikely that dust heated in such a manner can make a significant contribution to the mid-IR emission.

An additional possibility is that the dust could be heated via interaction with the hot plasma that has been postulated to give rise to the scattering of broad-line photons. Such effects are known to be important in supernova remnants (e.g., de Jong et al. 1990) and galaxy clusters (Bregman, McNamara, & O'Connell 1990). From comparison of the width of the broad lines scattered by the electron cloud with those scattered by dust, Miller et al. (1991) determine that the plasma is characterized by a temperature of $\sim 3 \times 10^5$ K. They also favor an electron density of $\sim$500 cm^{-3}, although this is less well con-

strained. The equilibrium temperature, T_d, that a dust grain of radius a (in μm) will attain in a plasma of density n_e and temperature T_p ($\leq 2 \times 10^7$ K) is given by (Dwek & Arendt 1992)

$$T_d \sim 0.6 n_e^{0.168} a^{-0.168} T_p^{0.252} . \quad (2)$$

For the electron cloud characteristics outlined above, even the smallest ($a \sim 0.001$ μm) dust grains internal to such a plasma would only achieve a temperature of ~ 130 K and would make a negligible contribution to the mid-IR emission.

3.3. *Dust Heated Directly by the Central Engine*

We now examine whether the observed mid-infrared emission could arise from dust heated directly by radiation from the central engine, in the same way that the gas in the narrow-line clouds is photoionized. For the moment we make no claim about the distribution or density of the dust, except that either it is mixed with the narrow-line clouds or it is located at the edges of the narrow-line region, or perhaps both. We begin with a first-order determination of the size of the region that could be heated by a source of luminosity L. Dust at a radius R from the central source will assume a characteristic temperature T, given by (Emerson 1988)

$$R \sim \left[\frac{Q_{\rm abs}(\rm opt) c^2}{32 a \pi^2 h Q_0 (3+n)!} L \left(\frac{kT}{h} \right)^{-(4+n)} \right]^{1/2} , \quad (3)$$

where $Q_{\rm abs}$(opt) is the dust absorption efficiency (ratio of the effective to the geometrical cross-sectional area) for UV and optical radiation, which is the wavelength domain principally absorbed by dust; Q_0 is a constant dependent only on the material, T is the grain temperature; and n is the coefficient of the power-law relationship between absorption efficiency and frequency. Draine & Lee (1984) have determined that $Q_{\rm abs}$(opt) is constant at close to unity over a large wavelength regime, and in the infrared $Q_0 \sim 2.8 \times 10^{-23}$. The value of the exponent is somewhat uncertain but appears to be ~ 1.6 in the 1 μm $< \lambda <$ 7 μm domain (Whittet 1988). Assuming an average grain size of 0.05 μm, equation (3) reduces to

$$R = 0.14 \left(\frac{L}{1.5 \times 10^{11} L_\odot} \right)^{0.5} \left(\frac{T}{1500 \text{ K}} \right)^{-2.8} \text{pc} . \quad (4)$$

Equation (4) suggests that dust particles that have a *direct view* of the central engine out to distances of ~ 100 pc will radiate principally in the mid-infrared. *Classical* interstellar dust is generally considered to be a mixture of silicate and graphite particles with grain sizes in the range 0.003–1.0 μm (Draine & Lee 1984). Recently, it has been realized that smaller particles made up of polycyclic aromatic hydrocarbons (PAHs), with radii ranging down to ~ 10 Å, may also play an important role in the interstellar medium (ISM) (Puget, Léger, & Boulanger 1985; Draine & Anderson 1985). Although such particles, lying within a few tens of parsecs of an AGN and exposed to its intense X-ray emission, are likely to be rapidly destroyed (Voit 1991), their presence at larger distances from the central engine could explain the observed highly extended nature of the mid-IR emission. Alternatively, if the nuclear radiation is beamed, then the luminosity of the nucleus would be larger than that estimated from infrared measurements. The ionization models of Miller et al. (1991) point to a bolometric luminosity several factors greater than the measured value. If this were the case, it could naturally explain the whole extent of the observed warm dust emission as a consequence of radiative heating by the nuclear source.

At $T \sim 1500$ K, graphites have a higher sublimation temperature than silicates, and this is likely to represent the highest temperature dust can achieve in any environment. From simple blackbody arguments, dust at temperatures in excess of 1000 K will radiate in the near-infrared, and thus significant column densities of dust lying within a few parsecs of the central engine of NGC 1068 should produce an *excess* emission feature in the 2–5 μm regime. Such a near-infrared bump is observed in the specrra of several quasars and AGNs (Robson et al. 1986) but not in NGC 1068 (Edelson & Malkan 1986). Since the peak energy output from the AGN in NGC 1068 occurs in the 10–20 μm wavelength range, with a corresponding temperature of ~ 400 K (Tresch-Fienberg et al. 1987), this would suggest that significant column densities of dust only become important at distances of ~ 5–10 pc from the source, depending on the dust particle size. This conclusion ignores the effects of radiative transfer in a dense, dusty structure, such as a torus, which could influence the shape of the output spectrum. Pier & Krolik (1992b) have taken such effects into account in their models of parsec-scale tori around AGNs and have demonstrated that such infrared excesses can only be concealed if the tori are viewed *exactly* edge-on. A deviation from an edge-on viewing angle of even $\sim 3°$ is sufficient to boost the near-infrared output dramatically. Unfortunately, the models of Pier & Krolik (1992b) are not entirely applicable to the case of NGC 1068, since the mass contained in their tori would only represent $\sim 10^{-3}$ of the total gas content of the central few hundred parsecs of NGC 1068. In addition, the molecular gas is known to be extended over several hundred parsecs (Cameron et al. 1993; Blietz et al. 1994; Tacconi et al. 1993). Rotaciuc et al. (1991) have argued that the excited H_2 emission, which has a different position angle from that of the narrow-line region and jet, is produced in warm gas heated by X-rays from the central source. The presence of a dense parsec-scale torus, the theoretical significance of which is to subtend a large solid angle with respect to the nucleus and additionally to present a barrier to high-energy photons in the X-ray–to–optical regime, would appear to be inconsistent with such a scenario.

4. CONSEQUENCES OF A DUSTY NARROW-LINE REGION

4.1. *Extinction and Scattering*

The most obvious role that dust could play in a NLR is that of an absorbing and scattering agent. The former presents a dilemma, since, while the measured visual extinction toward the narrow-line clouds is ~ 1.5 mag (Cecil et al. 1990), the column density of dust implied by our mid-infrared observations (see § 5) corresponds to a significantly greater attenuation ($A_V > 20$ mag). Since the dust is likely intimately linked with the narrow-line clouds seen in the optical, a particular geometry needs to be invoked in which the bulk of the warm dust lies behind those photoionized clouds that are visible. The most realistic way to arrange this is for the two emitting agents (i.e., that giving rise to the mid-infrared emission and that responsible for the photoionized clouds) to arise from the same bulk cloud material, such as discrete giant molecular clouds (GMCs), parts of which have a direct view of the central engine. Such clouds may be located at the interface between the cavity evacuated by the outflowing wind and the surrounding molecular disklike structure, and probably serve as a fuel supply for the AGN. The narrow-line clouds would then represent photoionized gas located at that side of a GMC which is

directly exposed to the intense radiation field of the AGN. Any line of sight to the NLR which dissects such a molecular cloud will be associated with high extinction, while clouds located at the conical surface farthest from us will only be visible if we have a relatively unobscured view of that surface of the cloud which has been ionized to form part of the NLR. The precise geometrical distribution of such clouds at the outflow/ISM interface should play an important role in determining the observable morphology of the NLR at high spatial resolution. A consequence of this model is that, *unless the angle between our line of sight and the axis of the conical cavity is small*, there should be optically bright ionized cloud surfaces which are concealed from us by those cooler, denser parts of the molecular cloud which lie in front. In reality, the opposite is observed to prevail: there are optical clouds with no apparent radio counterparts. Hence it seems that we have a favorable view of the interior of the cavity, consistent with the proposal of Miller et al. (1991) that the angle between our line of sight and the axis of the outflow cone is $\lesssim 30°$.

That scattering plays a role in the nuclear region of NGC 1068 has been clearly demonstrated by the observed level of polarization (Miller & Antonucci 1983; McLean et al. 1983; Antonucci & Miller 1985; Miller et al. 1991). Although electrons appear to be the dominant scattering agent, several observations have pointed to a possibly still significant role for dust (Miller & Antonucci 1983; Snijders, Netzer, & Boksenberg 1986; Bailey et al. 1988; Goodrich 1992). Any model must reconcile the lower degree of observed polarization of the narrow optical emission lines ($\sim 1\%$; Antonucci & Miller 1985; Goodrich 1992) with that of the nonstellar continuum ($\sim 16\%$; Antonucci & Miller 1985; Code et al. 1993). Since the narrow-line clouds which are visible are affected by relatively little extinction, the low level of polarization of the NLR is consistent with transmission of the light through the intervening interstellar dust (Whittet 1992), in which case no other local scattering agent is required. The observed level of polarization of the 10 μm emission ($\sim 1.4\%$; Aitken et al. 1984) suggests that some of the warm grains are aligned and that the dust emitting region must have a relatively high optical depth (Bailey et al. 1988). This is additional support for the proposal that only a small fraction of the dust seen in our 10.3 μm map is actually mixed with the optically visible narrow-line clouds, while the bulk of it is located deeper in the dusty molecular clouds, the surfaces of which form the NLR.

4.2. *Heating by Photoionization of Dust*

One of the difficulties encountered in recent years in attempts to model typical narrow-line regions has been the discrepancy between the electron temperature predicted by photoionization models and that determined from the measurements of certain line ratios, specifically He II $\lambda 4686/\mathrm{H}\beta$ and [O III] $(\lambda 5007 + \lambda 4959)/\lambda 4363$. The problem stems from the fact that photoionization models predict $T_e < 11{,}000$ K, whereas a range of 12,800 K $< T_e <$ 22,000 K is expected from observation of the above lines (Tadhunter, Robinson, & Morganti 1989). The [O III] $(\lambda 5007 + \lambda 4959)/\lambda 4363$ ratio in the inner ~ 20 pc of NGC 1068, which includes at least two of the prominent narrow-line clouds delineated by Evans et al. (1991), is 49 ± 8, corresponding to an electron temperature of 18,000 K (Caganoff et al. 1991). The temperature derived from this ratio is in good agreement with that implied by the C III $(\lambda 1907 + \lambda 1909)/\lambda 977$ and N III $\lambda 1750/\lambda 991$ ratios (Kriss et al. 1992). The additional heating effect, over that which would be expected from photoionization, has usually been attributed to shocks (e.g., Kriss et al. 1992) or cosmic-ray heating (Tadhunter et al. 1989).

However, Magris, Binette, & Martin (1992) and Netzer & Laor (1993) have recently demonstrated that the mixing of dust with narrow-line clouds can significantly enhance the expected electron temperature by typically $\sim 50\%$ via photoionization of the dust. It is likely that this additional heating effect of the dust which is associated with the NLR, and which is clearly delineated by our mid-infrared observations, could account for the temperature deduced from the UV and optical line ratios. Dust heating in this context only becomes important in the presence of large values of U, the ionization parameter defined as the ratio of the ionizing photon density to the gas density. In this case, the recombination of electrons on grains, which cools the gas, is less significant than the photoelectric heating contribution. In addition, although the cross section for grain photoionization is smaller than that of hydrogen, under conditions of high U when the hydrogen becomes highly transparent to the radiation field, the photoionization rate of the dust is comparable to that of the gas. It is at this point that grain photoheating becomes important. The reason for this is that dust particles can withstand numerous ionization events, of the order of $\sim 10^2$, without drastically increasing their ionization potential (Binette 1993). Thus it would appear that dust may play an important role in the thermal balance in such photoionized regions. However, as already discussed, it is unlikely that the majority of the dust seen in our 10.3 μm image is actually mixed in with the narrow-line clouds. These clouds are bathed in an extremely hard radiation field, possibly resulting in the destruction of large quantities of dust mixed with the gas. This is consistent with the dusty photoionization models of Binette, Magris, & Martin (1992), which require only ~ 2 mag of dust to be mixed with the gas.

Dust forming a foreground attenuating screen to a cloud of emitting gas and dust actually mixed with the gas represent two situations which require different treatments when determining the level of extinction from observed line ratios. The former case is relatively simple, since the dust screen attenuates line emission (used as an extinction diagnostic) in a way described by appropriate extinction curves. However, this is not the case for dust embedded in a cloud giving rise to line emission, since the strength of lines emitted by different species at different depths in the cloud will be modified by differential extinction (Netzer & Loar 1993). In such a situation line ratios become less sensitive to the prevailing extinction and may result in ambiguous estimates.

4.3. *Distribution of Warm Dust versus Distribution of Gas*

One obvious question that needs to be confronted is why the distribution of the mid-infrared emission is so different from that of the warm molecular gas. The position angle of the former is displaced by $\sim 55°$ relative to that of the latter, yet we have proposed that both are the result of extinction by radiation from the central engine. The solution to this apparent problem may lie in the presence of the conical cavity which has its axis along the position of the radio jet. A crucial point to recall is that the projected area occupied by the warm dust is merely a subset of that in which the molecular gas is located. X-ray emission from the AGN has been proposed as the mechanism most likely to be responsible for heating the gas and thereby giving rise to the observed H_2 emission (Rotaciuc et al. 1991). Typical mixtures of silicate and graphite particles

assumed to represent the composition of dust in our own Galaxy (Mathis, Rumpl, & Nordsieck 1977) are characterized by absorption cross sections which are an order of magnitude greater for UV ($\lambda = 1000$ Å) than for soft X-rays ($h\nu = 0.5$ keV), and several orders of magnitude greater than for harder photons (Laor & Draine 1993). This implies that X-ray photons will penetrate significantly farther into a dusty disk than UV photons, offering a possible explanation for the different spatial morphologies between the mid-IR map and that of the H_2 distribution: UV continuum photons are absorbed by dust particles at relatively small distances from the central source, while X-rays, which at these energies do not differentiate between atoms bound in a solid particle and those in the gas phase (Krolik 1992), penetrate much farther into the molecular disk but are as likely to heat the gas as the dust. However, the fact that the outflow cavity appears to be relatively dust-free will allow optical and UV photons to escape much farther along the direction delineated by the NLR, compared with their free path length along the major axis of the disk, before they are absorbed by the dusty molecular clouds which form the boundary layer.

5. AN ALTERNATIVE MODEL FOR NGC 1068

The fact that only ~30%–40% of the mid-IR emission is emitted in the direct vicinity of the nucleus requires that any parsec-scale torus has an opening angle of ~138°, far greater than that supported by tracing out the shape of the outflow cone (Evans et al. 1991; Pogge 1988). This estimate would be somewhat erroneous if the emission from the nucleus were intrinsically beamed, in which case the luminosity of the nucleus could be larger than observed (Miller et al. 1991). In addition, if the highly spatially extended distribution of warm molecular gas is the result of excitation in X-ray–heated gas (Rotaciuc et al. 1991), then radiation from the central engine must penetrate several hundred parsecs into the circumnuclear ISM along the direction in which the proposed dense torus is supposed to lie. Furthermore, it is now clear that the absence of a near-IR excess in the nuclear spectrum of NGC 1608 (Edelson & Malkan 1986) is consistent with the presence of a parsec-scale dense molecular structure only if that torus is seen *exactly* edge-on (Pier & Krolik 1992b). In § 3 we argued, using relatively simple formulisms, that large column densities of very hot dust are unlikely to lie within a few parsecs of the nucleus of NGC 1068. Thus, any torus in the nuclear vicinity could not have a radius ≤ 5 pc, at which point it would cease to fulfill the absorbing and containment roles proposed for it (Krolik 1989). Such observational evidence weakens the case for the necessity of a dusty parsec torus enclosing the BLR. As a means of circumventing the need for such a torus altogether, we have developed an alternative model which, while accounting for the obscuration of the broad-line region does not include a significant concentration of molecular material in the inner few parsecs. We now proceed to describe this scenario in depth and present results of a detailed radiative transfer calculation.

5.1. *The Absent-Torus Scenario*

The main points of our model are illustrated in Figure 5, which is a schematic view of the possible distribution of material out to a radius of a few hundred parsecs from the nucleus. The nucleus is surrounded by a small-scale ($\ll 1$ pc) radiation torus which is probably responsible for the nonthermal emission of the AGN. We envisage that the disklike structure surrounding the AGN, seen in images of excited H_2, is made up of giant molecular clouds with characteristics not dissimilar to those in our own galaxy, except that they may be somewhat more highly compressed owing to their location close to a strong gravitational field (Krolik & Begelman 1986). We assume that the dust density scales with radius as $n \propto R^{-\beta}$, where β was initially a free parameter. In order to minimize the amount of matter close to the nonthermal continuum source, we chose a range of values $0 \leq \beta \leq 1$, and, after several model runs, we fixed β so that the dust density scales as $R^{-0.5}$ between 5 and 200 pc. Thus the amount of dust increases with $R^{2.5}$ for a spherically symmetrical distribution or with $R^{1.5}$ in the case of a flattened disklike structure. This configuration has the effect that the bulk of the molecular material lies at large radii from the nucleus. Since there is no torus in this model, radiation from the AGN can escape isotropically unless it is beamed by some mechanism that operates on relatively small scales. This means that photons can penetrate the body of the molecular cloud distribution, heating the gas via the absorption of X-rays and exciting the H_2 sufficiently to allow it to radiate in the 2.121 μm line. Photons which escape along the conical cavity travel farther and, as outlined in the previous section, are additionally responsible for heating the dust in clouds at the outflow/ISM boundary. Gas in these molecular clouds that has a direct view of the AGN, and is thus photoionized, would then form the narrow-line clouds. The severe attenuation along our line of sight to the broad-line region could then be the result of one or more intervening molecular clouds. Krolik & Begelman (1986) argue that a single such cloud would be sufficient to provide complete shielding of the nuclear radiation.

5.2. *The Numerical Model*

Using a radiative transfer code for clouds containing radiatively heated dust particles described by Siebenmorgen, Krügel, & Mathis (1992) and Siebenmorgen (1993), but modified for the particular requirements of a AGN environment, we have calculated the spectrum from the model detailed above as well as one incorporating a parsec-scale torus. Since the numerical method is fully discussed in the above references, here we restrict ourselves to a brief description of the more important elements. We stress that, since the code can only deal with spherically symmetric dust distributions, the results we present here should be treated as merely an approximation of the situation prevailing in the inner few hundred parsecs of NGC 1068.

In the dust model of Siebenmorgen & Krügel (1992) the dust grains are assumed to have a power-law size distribution given by $n(a) \propto a^{-q}$, where a is the grain radius and q is a constant depending on the dust type. The various dust formats incorporated in this model are the following:

1. Large grains with radii ranging between 300 and 1200 Å for amorphous carbon and silicates for which $q = 3.5$.
2. Small graphite grains with 10 Å $\leq a \leq$ 100 Å and $q = 4$, assumed to be responsible for the 2175 Å bump (Draine 1989).
3. A population of PAHs, responsible for emission features in the near- and mid-infrared (Puget & Léger 1989; Allamandola, Tielens, & Barker 1989). Two varieties of PAHs are included in our model calculation: small molecules comprising 25 atoms and larger clusters of 10 such molecules.

The interstellar extinction curve of Mathis (1990) has been assumed to characterize the large grains and small graphites.

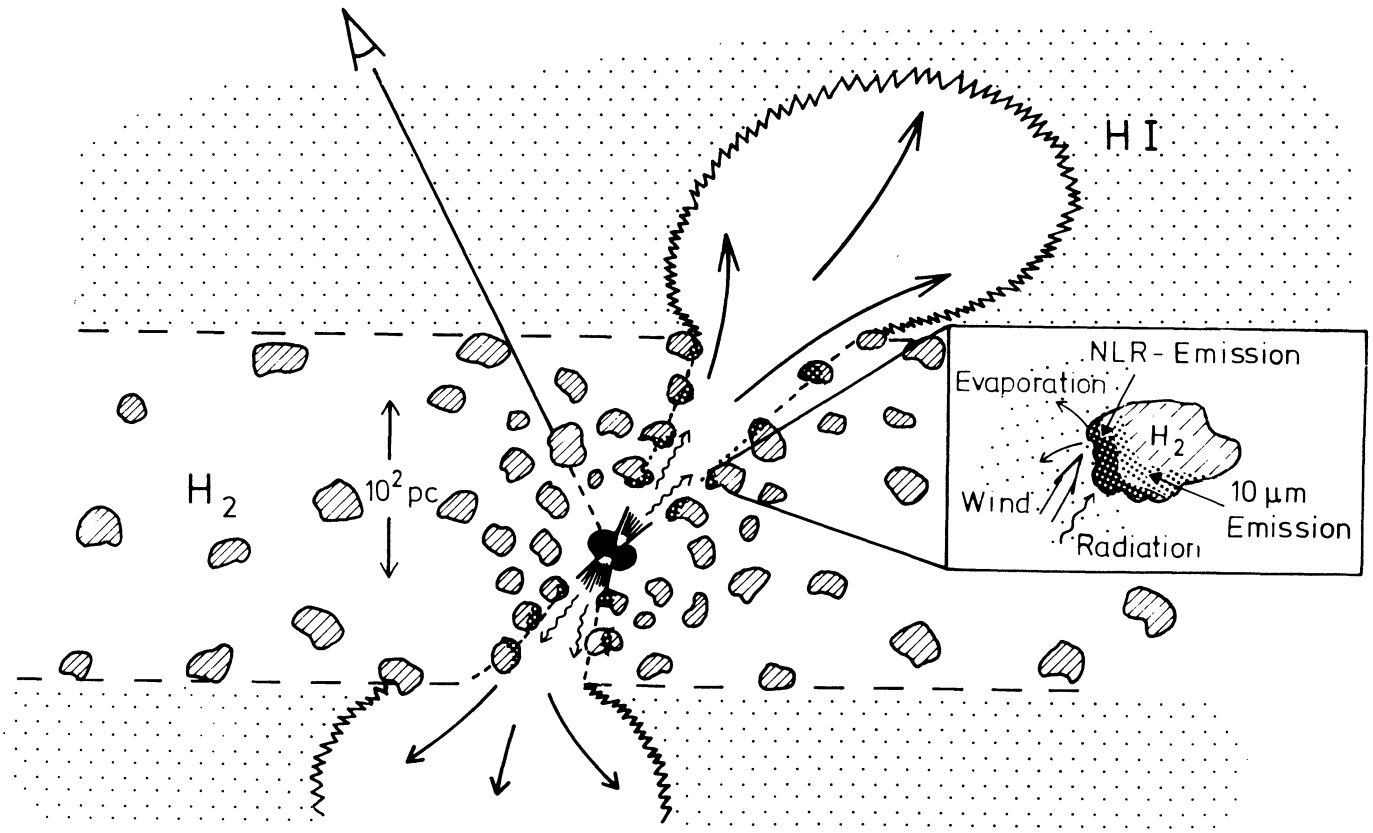

FIG. 5.—Schematic illustrating the distribution of material in the inner few hundred parsecs of NGC 1068 as envisaged in the *absent-torus* model. The observer's view of the broad-line region is obscured by one or more molecular clouds located in the extended circumnuclear disk. The narrow-line region represents the exposed surfaces of molecular clouds which lie at the outflow cone/ISM interface and which are bathed in the intense radiation field of the AGN. The bulk of the mid-infrared is emitted by warm dust internal to these clouds. The lack of material in the disk to the south of the AGN explains the observed asymmetry in the mid-infrared and radio maps.

The fractional abundance of the small graphites and PAHs relative to solid carbon has been set at 0.15 and 0.067, respectively. The number of hydrogen atoms relative to carbon atoms making up the PAHs (the hydrogenation parameter) is 0.2. An important element in this radiative transfer calculation is the inclusion of scattering effects and the photodestruction of small dust particles due to multiple photon-grain interactions in the innermost part of the dust shell. Only the larger grains contribute to scattering, but all grain types/sizes play a role in extinction.

The source function, S_ν, is given by

$$\kappa_\nu^{\rm ext} S_\nu = \Gamma_\nu + \sum_l \left[\kappa_{\nu,l}^{\rm sca} J_\nu + \kappa_{\nu,l}^{\rm abs} \int B_{\nu,l}(T) P_l(T) dT \right], \quad (5)$$

where l denotes the various dust particle types/sizes, $B_{\nu,l}(T)$ is the Planck function, $P_l(T)$ is the temperature distribution function, $\kappa_\nu^{\rm ext}$ is the sum of the absorption ($\kappa_\nu^{\rm abs}$) and scattering ($\kappa_\nu^{\rm sca}$) cross sections respectively, and $\Gamma_\nu \propto \nu^{-\alpha}$, where $\int \Gamma \, d\nu = L = 1.74 \times 10^{11} \; L_\odot$. The input spectrum was assumed to be a power law with an index of $\alpha = -2.0$ as determined by Edelson & Malkan (1986) for NGC 1068.

5.3. *Model Results*

The method described in the previous section was applied to two distributions of dust about an AGN. The first, the *absent-torus scenario*, consists of a spherically symmetrical shell with an inner edge located at a radius of 5 pc and an outer boundary at 200 pc. The average number density at the inner edge of this shell is 700 cm^{-3}. In addition, we have run separate model calculations in which a torus-like structure is included. In this case we assume a structure of number density 5000 cm^{-3} which has inner and outer radii of 0.5 and 1.5 pc, respectively (representing the torus), with a less dense shell extending out to 200 pc. After several attempts to optimize the torus model, it became clear that a continuous distribution of material, extending from 0.5 pc, overestimated the emission in the near-IR. As a means of rectifying this, we were forced to introduce a discontinuity in the molecular cloud distribution, such that little material is present between 1.5 and 5 pc. It should be noted that the absent-torus model is merely a subset of the torus model, with the only difference being that the inner dense shell is not present in the former. In both cases the total mass of gas and dust being illuminated by the central engine is $\sim 1.5 \times 10^8 \; M_\odot$ (the mass of the torus structure is small compared with the mass in the outer shell). It should be emphasized at this point that the distributions modeled here do not strictly adhere to the torus and absent-torus cases envisaged in the previous sections. This discrepancy is primarily due to deviations from the spherical symmetry that is an inherent characteristic of the radiative transfer code and the fact that no outflow cone is incorporated. However, we believe that the results of our model runs should be representative of the two cases, provided that both the disklike structure (containing the bulk of the molecular gas and dust) and the torus are observed

close to edge-on. These constraints would appear to be consistent with the elongation of the extended excited H_2 seen at 2.121 μm and the requirements of torus calculations (Pier & Krolik 1992b). One problem with a spherically symmetric dust distribution is that the total mass in a shell equivalent to the observed column density of gas in a flattened disk structure (seen essentially edge-on) should be greater than that actually measured for NGC 1068. This explains the factor of 5 enhancement of the gas mass determined here over that measured by Planesas et al. (1991).

Figure 6 shows the results of two best fits for both of these cases. One deficiency with the absent-torus model fit is that it does not fully match the observed depth of the silicate absorption feature. It is likely that this is a consequence of the fact that the model does not incorporate discrete clouds but rather assumes a homogeneous distribution of cloud material. Except at the wavelength extremes, both models appear to fit the observed spectrum reasonably well. The poor fit in the near-IR can probably be attributed to the contribution of stellar light, while the large beam sizes characteristic of far-IR data make it extremely difficult to distinguish between material in the nuclear vicinity and that present in the surrounding starburst ring. However, the good fit we obtain to the data in both the absent-torus and the torus cases suggests that the presence of a torus is not an essential requirement in fitting the observed spectrum of the nucleus of NGC 1068. Indeed, the fact that a torus model does not allow a deviation from an edge-on geometry (Pier & Krolik 1992b), and that, in the case of the model presented here, it requires a discontinuity in the distribution of gas and dust between 1.5 and 5 pc to prevent the appearance of a near-IR bump, raises the prospect that such a structure may not exist, at least in the form currently envisaged in the unifying model. The column density of material associated with the line of sight to the nucleus corresponds to visual extinctions of $A_V = 26$ and $A_V = 134$ in the case of the absent-torus and torus-included models, respectively. Obviously, because of the homogeneous distribution of material assumed by our model, these numbers should be regarded as lower limits because of the undoubtedly clumpy nature of the actual molecular distribution.

One intriguing difference between these models is highlighted in Figure 6, namely, the predicted presence of PAH features in the spectrum emitted in the case of the absent-torus model but their absence in that from the torus model. This arises because the dense material in the torus is, due to its closeness to the AGN, bathed in such an intense radiation field that the PAH particles are rapidly destroyed. Little hard radiation can penetrate the torus and excite the PAHs in the 5–200 pc disk. In the absent-torus model, X-ray and UV photons can reach the outer shell, but at these distances from the AGN the radiation field has been sufficiently diluted that few PAHs are destroyed. However, the incident flux from the central source is still sufficient to promote nonequilibrium heating in these small particles, producing strong emission in the 3.3 and 11.3 μm bands. Unfortunately, no data obtained with a sufficiently small beam to avoid contamination by neighboring star-forming regions are available for the nuclear region in NGC 1068. This, however, could be used as a possible test of the likely distribution of material in the inner few hundred parsecs.

These results demonstrate that a model which is based on a continuous distribution of material, but which does not incorporate large column densities of material lying close to the AGN, is at least as applicable to NGC 1068 as one incorporating a torus. One aspect of the torus model which cannot be matched by our absent-torus scenario is the role the former supposedly plays in the collimation of the nuclear outflow (Krolik & Begelman 1986). However, Miller et al. (1991) have argued that it is unlikely in any case that a parsec-scale torus could be responsible for the observed level of the collimation. In the alternative model presented here we assume that such collimation either occurs on very small spatial scales close to the AGN or is a consequence of the molecular cloud distribution which forms a natural buffer zone along the outflow cone.

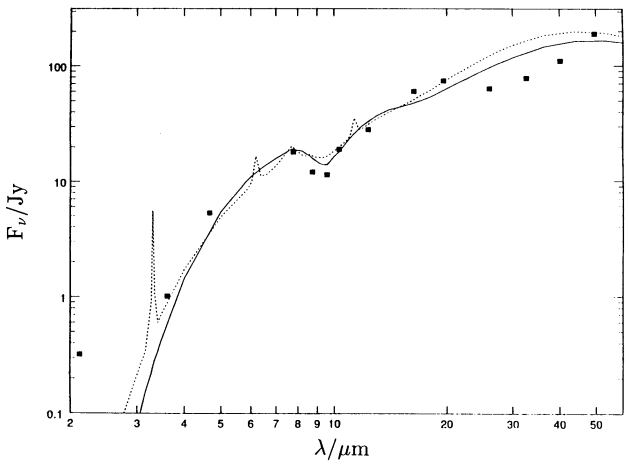

FIG. 6.—Results of model-fitting the observed spectrum of the nuclear region of NGC 1068 using a radiative transfer code for dusty clouds. The dotted line represents the *absent-torus* model of an extended (5–200 pc) dusty disk in which the number density scales as $R^{-0.5}$. The solid line represents a model which *additionally* incorporates a parsec-scale torus consisting of a dense shell, the inner and outer radii of which are positioned at 0.5 and 1.5 pc, respectively, from the AGN.

6. SUMMARY

1. Imaging of the 10.3 μm emission in the nuclear vicinity of NGC 1068 reveals that warm dust is extended over $\sim$140 pc, and although an emission maximum, probably coincident with the nucleus, is present, it does not dominate the energy output from the region.

2. Comparison of our deconvolved 10.3 μm images with *HST* data, both at angular resolutions of 0".5 or better, reveals a striking spatial correspondence between the warm dust and the narrow-line clouds. This strongly suggests that large column densities of dust are physically associated with the narrow-line region, but, although partially mixed with the photoionized clouds, the bulk of the warm dust is located in molecular clouds at the outflow/ISM interface.

3. The scenario that the dust could be heated in extended star formation regions by shocks, or via collisions in a hot plasma does not appear to be consistent with the fact that the warm dust pervades a region of $\sim$140 pc in extent. Rather, we argue that the dust is more likely heated by radiation from the central source.

4. The observation of dust mixed with the NLR, although only likely to correspond to an extinction of a few magnitudes, apparently resolves one of the major discrepancies between the measured electron temperatures in photoionized clouds and those predicted by dust-free models. Electrons released in photoionization of grains are responsible for an increase in the gas temperature.

5. These and a number of other observations cast doubt on aspects of current unifying theories which incorporate parsec-scale dusty tori. We have therefore proposed an alternative model in which the bulk of the molecular gas and dust is located at large distances (several tens of parsecs) from the AGN. Line-of-sight attenuation of the BLR in this case would be a mere consequence of one or more intervening molecular clouds. Using a radiative transfer model for dusty clouds, which includes consideration of scattering by grains, we have demonstrated that the spectrum of the nuclear environment of NGC 1068 can be fitted equally well with models both incorporating and excluding a dense, dusty few-parsec-scale torus. However, in order to prevent the appearance of an infrared excess in the case of the torus model, the molecular cloud distribution, which is known to extend out to a radius of ~ 140 pc, must include a discontinuity of several parsecs between the torus and the gas in the extended disk.

6. Our analysis suggests that the strength of the near- and mid-IR bands due to emission from PAHs could be used as a test to differentiate between these these two cases. Provided that there were no contamination from star-forming regions in the inner 5″, our model calculations predict that these bands would be observable only in the absence of a dense, dusty torus.

It is a pleasure to acknowledge the MPE, ROE, and UKIRT personnel who ensured that the MIRACLE project was commissioned on relatively short timescales. In particular, we are grateful to Alfred Krabbe, Wolfgang Heigl, and Georg Sämann (MPE), Andy Longmore (ROE), and Colin Aspin, Tom Geballe, and Phil Williams (UKIRT) for their help with all aspects of the project and their enthusiastic support. We are indebted to Ian Evans and his collaborators who kindly made available their deconvolved *HST* image of the narrow-line region. We thank Andreas Eckart for advice on the use of his deconvolution algorithm, and Luc Binette for valuable discussions on various aspects of his photoionization models. J. W. V. S. is grateful to the Alexander von Humboldt Stiftung and DITAC (Australia) for their support.

REFERENCES

Aitken, D. K., Bailey, J. A., Briggs, G., Hough, J. H., & Roche, P. F. 1984, Nature, 310, 660
Allamandola, L. J., Tielens, A. G. G. M., & Barker, J. R. 1989, ApJS, 71, 733
Antonucci, R. R. J. 1992, in AIP Conf. Proc., Vol. 254, Testing the AGN Paradigm, ed. S. S. Holt, S. G. Neff, & C. M. Urry (New York: AIP), 486
Antonucci, R. R. J., & Miller, J. S. 1985, ApJ, 297, 621
Atherton, P. D., Reay, N. K., & Taylor, K. 1985, MNRAS, 216, 17P
Awaki, H., Koyama, K., Inoue, H., & Halpern, J. P. 1991, PASJ, 43, 195
Bailey, J., Axon, D. J., Hough, J. H., Ward, M. J., McLean, I., & Heathcote, S. R. 1988, MNRAS, 234, 899
Baldwin, J. A., Wilson, A. S., & Whittle, M. 1987, ApJ, 319, 84
Balick, B., & Heckman, T. 1985, AJ, 90, 197
Bally, J., Stark, A. A., Wilson, R. W., & Henkel, C. 1987, ApJS, 65, 13
Balsara, D. S., & Krolik, J. H. 1993, ApJ, 402, 109
Becklin, E. E., Matthews, K., Neugebauer, G., & Wynn-Williams, C. G. 1973, ApJ, 186, L69
Binette, L. 1993, private communication
Binette, K., Magris, C. G., & Martin, P. G. 1993, in Proc. Conf. on First Light in the Universe: Stars or QSOs?, ed. B. Volmerange et al. (Gif-sur-Yvette: Editions Frontières), 243
Blietz, M., Cameron, M., Drapatz, S., Genzel, R., Krabbe, A., van der Werf, P. P., Sternberg, A., & Ward, M. J. 1994, ApJ, in press
Braatz, J. A., Gezari, D. Y., Varosi, F., & Wilson, A. S. 1992, BAAS, 24, 728
Bregman, J. N., McNamara, B. R., & O'Connell, R. W. 1990, ApJ, 351, 406
Bruhweiler, F. C., Truong, K. Q., & Altner, B. 1991, ApJ, 379, 596
Caganoff, S., et al. 1991, ApJ, 377, L9
Cameron, M., et al. 1993, in Proc. Third Teton Summer School on the Evolution of Galaxies and Their Environment, ed. D. Hollenbach, H. Thronson, & J. M. Shull (NASA CP-3190), 315
Cameron, M., Storey, J. W. V., Rotaciuc, V., Genzel, R., Drapatz, S., Krabbe, A., Verstraete, L., & Lee, T. 1992, in Proc. ESO Conf. and Workshop, Vol. 42, Progress in Telescope and Instrumentation Technologies, ed. M.-H. Ulrich (Garching: ESO), 705
Cardelli, J. A., Clayton, G. C., & Mathis, J. S. 1989, ApJ, 345, 245
Cecil, C., Bland, J., & Tully, R. B. 1990, ApJ, 355, 70
Chelli, A., Perrier, C., Cruz-González, I., & Carrasco, L. 1987, A&A, 177, 51
Code, A. D., et al. 1993, ApJ, 403, L63
Cutri, R. M., et al. 1981, ApJ, 245, 818
de Jong, T., Nørgaard-Nielsen, H. U., Jørgensen, H. E., & Hansen, L. 1990, A&A, 232, 317
DePoy, D. L. 1987, in Proc. Workshop on Ground-based Astronomical Observations with Infrared Detectors, ed. C. G. Wynn-Williams & E. E. Becklin (Honolulu: Univ. Hawaii), 426
Draine, B. T. 1981, ApJ, 245, 880
———. 1989, IAU Symp. 135, Interstellar Dust, ed. L. Allamandola & A. G. G. M. Tielens (Dordrecht: Kluwer), 313
Draine, B. T., & Anderson, N. 1985, ApJ, 292, 494
Draine, B. T., & Lee, H. M. 1984, ApJ, 285, 89
Dwek, E., & Arendt, R. G. 1992, ARA&A, 30, 11
Edelson, R. A., & Malkan, M. A. 1986, ApJ, 308, 59
Elvis, M., & Lawrence, A. 1988, ApJ, 331, 161
Emerson, J. P. 1988, in NATO ASI Ser. C, Vol. 241, Formation and Evolution of Low Mass Stars, ed. A. K. Dupree & M. T. V. T. Lago (Dordrecht: Kluwer), 21
Evans, I. N., Ford, H. C., Kinney, A. L., Antonucci, R. R. J., Armus, L., & Caganoff, S. 1991, ApJ, 369, L27
Fischer, J., Smith, H. A., & Glaccum, W. 1991, in ASP Conf. Ser., Vol. 14, Astrophysics with Infrared Arrays, ed. R. Elston (San Francisco: ASP), 63
Gallais, P. 1991, Ph.D. thesis, Univ. Paris VII
Genzel, R., Cameron, M., & Krabbe, A. 1992, in Proc. Madrid Conf. on the Nearest Active Galaxies, ed. J. Beckman & L. Colina, in press
Goodrich, R. W. 1992, ApJ, 399, 50
Hofmann, R., et al. 1993, in preparation
Keto, E., Ball, R., Arens, J., Jernigan, G., & Meixner, M. 1992, ApJ, 387, L17
Kleinmann, D. E., Gillett, F. C., & Wright, E. L. 1976, ApJ, 208, 42
Koski, A. T. 1978, ApJ, 223, 56
Kriss, G. A., Davidsen, A. F., Blair, W. P., Ferguson, H. C., & Long, K. S. 1992, ApJ, 394, L37
Krolik, J. H. 1989, in Proc. of the 23d ESLAB Symp., X-Ray Astronomy. 2. AGN and the X-Ray Background, ed. J. Hunt & B. Battrick (Paris: ESA), 777
———. 1992, in AIP Conf. Proc. Vol. 25, Testing the AGN Paradigm, ed. S. S. Holt, S. G. Neff, & C. M. Urry (New York: AIP), 473
Krolik, J. H., & Begelman, M. C. 1986, ApJ, 308, L55
———. 1988, ApJ, 329, 702
Laor, A., & Draine, B. T. 1993, ApJ, 402, 441
Lawrence, A. 1991, MNRAS, 252, 586
Lebofsky, M. J., Rieke, G. H., & Kemp, J. C. 1978, ApJ, 222, 95
Lucy, L. B. 1974, AJ, 79, 745
Lynds, R., et al. 1991, ApJ, 369, L31
Magris, C. G., Binette, L., & Martin, R. G. 1992, in Proc. Madrid Conf. on the Nearest Active Galactic Nuclei, ed. J. Beckman & L. Colina, in press
Mathis, J. S. 1990, ARA&A, 28, 37
Mathis, J. S., Rumpl, W., & Nordsieck, K. H. 1977, ApJ, 215, 425
McLean, I. S., Aspin, C., Heathcote, S. R., & McCaughrean, M. J. 1983, Nature, 304, 609
Meaburn, J., Morgan, B. L., Vine, H., Pedlar, A., & Spencer, R. 1982, Nature, 296, 331
Miller, J. S., & Antonucci, R. R. J. 1983, ApJ, 271, L7
Miller, J. S., Goodrich, R. W., & Mathews, W. G. 1991, ApJ, 378, 47
Monier, R., & Halpern, J. P. 1987, ApJ, 315, L17
Mulchaey, J. S., Mushotzky, R. F., & Weaver, K. A. 1992, ApJ, 390, L69
Netzer, H. 1990, in Saas-Fée Advanced Course, Active Galactic Nuclei, Vol. 20, ed. T. J. L. Courvoisier & M. Mayor (Berlin: Springer), 57
Netzer, H., & Laor, A. 1993, ApJ, 404, L51
Osterbrock, D. E. 1991, Rev. Progr. Phys., 54, 579
Phinney, E. S. 1989, in NATO ASI Series C, Vol. 290, Theory of Accretion Disks, ed. F. Meyer et al. (Dordrecht: Kluwer), 457
Pier, E. A., & Krolik, J. H. 1992a, ApJ, 399, L23
———. 1992b, ApJ, 401, 99
Piña, R. K., Jones, B., Puetter, R. C., & Stein, W. A. 1992, ApJ, 401, L75
Planesas, P., Scoville, N., & Myers, S. T. 1991, ApJ, 369, 364
Pogge, R. W. 1988, ApJ, 328, 519
Puget, J. L., & Léger, A. 1989, ARA&A, 27, 161
Puget, J. L., Léger, A., & Boulanger, F. 1985, A&A, 142, L19
Richardson, W. H. 1972, J. Opt. Soc. Am., 62, 55
Robson, E. I., Gear, W. K., Brown, L. M. J., Courvoisier, T. J.-L., Smith, M. G., Griffin, M. J., & Blecha, A. 1986, Nature, 323, 134

Roche, P. F., Aitken, D. K., Phillips, M. M., & Whitmore, B. 1984, MNRAS, 207, 35
Roche, P. F., Aitken, D. K., Smiyh, C. H., & Ward, M. J. 1991, MNRAS, 248, 606
Rotaciuc, V., Krabbe, A., Cameron, M., Drapatz, S., Genzel, R., Sternberg, A., & Storey, J. W. V. 1991, ApJ, 370, L23
Sandage, A., & Tammann, G. 1981, Revised Shapley-Ames Catalog of Bright Galaxies (Washington, DC: Carnegie Inst. Washington)
Scoville, N. Z., Matthews, K., Carico, D. P., & Sanders, D. B. 1988, ApJ, 327, L61
Siebenmorgen, R. 1993, ApJ, 408, 218
Siebenmorgen, R., & Krügel, E. 1992, A&A, 259, 614
Siebenmorgen, R., Krügel, E., & Mathis, J. S. 1992, A&A, 266, 501
Snijders, M. A. J., Netzer, H., & Boksenberg, A. 1986, MNRAS, 222, 549
Sokolowski, J., Bland-Hawthorn, J., & Cecil, G. 1991, ApJ, 375, 583
Storchi-Bergmann, T., Mulchaey, J. S., & Wilson, A. S. 1992, ApJ, 395, L73
Tacconi, L. J., et al. 1993, in preparation
Tadhunter, C. N., Robinson, A., & Morganti, R. 1989, in Proc. ESO Conf. and Workshop, Vol. 32, Extranuclear Activity in Galaxies, ed. E. J. A. Meurs & R. A. E. Fosbury (Garching: ESO), 293
Tamura, M., Kleinmann, S. G., Scoville, N. Z., & Joyce, R. R. 1991, ApJ, 371, 131
Telesco, C. M., Becklin, E. E., Wynn-Williams, C. G., & Harper, D. A. 1984, ApJ, 282, 427
Telesco, C. M., & Decher, R. 1988, ApJ, 334, 573
Telesco, C. M., & Gezari, D. Y. 1992, ApJ, 395, 461
Telesco, C. M., & Harper, D. A. 1980, ApJ, 235, 392
Tresch-Fienberg, R., Fazio, G. G., Gezari, D. Y., Hoffmann, W. F., Lamb, G. M., Shu, P. K., & McCreight, C. R. 1987, ApJ, 312, 542
Tully, R. B. 1988, Nearby Galaxies Catalog (New York: Cambridge Univ. Press)
Ulvestad, J. S., Neff, S. G., & Wilson, A. S. 1987, AJ, 93, 22
Unger, S. W., Lewis, J. R., Pedlar, A., & Axon, D. J. 1992, MNRAS, 258, 371
van der Hulst, J. M., Hummel, E., & Dickey, J. M. 1982, ApJ, 261, L59
Veilleux, S., & Osterbrock, D. E. 1987, ApJS, 63, 295
Viegas-Aldrovandi, S. M., & Contini, M. 1989, ApJ, 339, 689
Voit, G. M. 1991, ApJ, 377, 158
Whittet, D. C. B. 1988, in Dust in the Universe, ed. M. E. Bailey & D. A. Williams (New York: Cambridge Univ. Press), 28
———. 1992, in Dust in the Galactic Environment, ed. R. J. Tayler & R. E. White (Bristol: IOP)
Wilson, A. S., Elvis, M., Lawrence, A., & Bland-Hawthorn, J. 1992, ApJ, 391, L75
Wilson, A. S., & Ulvestad, J. S. 1983, ApJ, 275, 8
———. 1987, ApJ, 319, 105
Wynn-Williams, C. G., Becklin, E. E., & Scoville, N. Z. 1985, ApJ, 297, 607